Microstructural changes in cartilage and bone related to repetitive overloading in an equine athlete model

Sean Turley, Ashvin Thambyah, Neil Broom

Experimental Tissue Mechanics Laboratory, Department of Chemical and Materials Engineering, University of Auckland

ABSTRACT

The palmar aspect of the third metacarpal condyle (MC3) of equine athletes is known to be subjected to repetitive overloading that can lead to the accumulation of joint tissue damage, degeneration, and even catastrophic fracture. However, there is still a need to understand at a detailed microstructural level how this damage progresses in the context of the wider joint tissue complex, i.e. the articular surface, the hyaline and calcified cartilage, and the subchondral bone. MC3 bones from non-fractured joints were obtained from the right forelimbs of 16 Thoroughbred athletes varying in age between 3 and 8 years, and with documented histories of active race training. Detailed microstructural analysis of two clinically important sites, the parasagittal groove and the mid-condylar region, identified extensive levels of microdamage in the calcified cartilage and subchondral bone concealed beneath outwardly intact hyaline cartilage. The study shows a progression in microdamage severity, commencing with mild hard-tissue microcracking in younger animals and escalating through to severe subchondral bone collapse and lesion formation in the hyaline cartilage with increasing age. The presence of a clearly distinguishable fibrous tissue layer at the articular surface immediately above sites of severe subchondral collapse suggested a limited reparative response in the hyaline cartilage.

Key words: Equine athlete; MC3; overload arthrosis; microdamage; subchondral bone; calcified cartilage; hyaline cartilage; repair.

INTRODUCTION

Excessive mechanical loading such as repetitive impact is known to lead to the formation of microcracks in both the subchondral bone (Radin, Parker et al. 1973; Zioupos and Currey 1994; Martin, Stover et al. 1996) and calcified cartilage (Mori, Harruff et al. 1993; Sokoloff 1993). With continued loading crack density increases if the remodelling response is unable to keep pace with the rate of new crack formation (Schaffler, Radin et al. 1989; Mori, Harruff et al. 1993; Martin, Stover et al. 1996). High levels of microdamage, interacting with the complex biological responses of the osteochondral tissues, can lead to the formation of much larger scale 'stress' fractures (Riggs 2002), or to degeneration and, ultimately, loss of the overlying articular cartilage (Burr and Radin 2003).

The palmar aspect of the third metacarpal condyle (MC3) of equine athletes is a region subjected to repetitive trauma and high bone strains (Biewener 1993), conditions which can lead to an accumulation of microdamage and eventually to a loss of joint health. One manifestation of microdamage-induced pathology in this region is known as palmar osteochondral disease (POD), which is believed to result from the repetitive cyclical over-extension of the metacarpophalangeal joint associated with high intensity exercise (Pool 1996; Norrdin, Kawcak et al. 1998). This condition may be classified as a form of 'overload arthrosis', with similar conditions also found in human athletes and joggers, and in those affected by obesity or joint malalignment (Frost 1994).

POD lesions appear as focal sites of subchondral bone failure and occur at consistent locations on either the lateral or medial condyles (Pool 1996), in a well-defined region of the joint known to experience very high *in vivo* loading during high speed locomotion (Biewener, Thomason et al. 1983). The earliest sign of POD is a bruising of the subchondral bone, which is visible through the still intact hyaline cartilage. Later stages of the disease involve subchondral bone disruption accompanied by varying levels of cartilage degeneration, leading ultimately to subchondral bone collapse and ulceration of the cartilage (Riggs 2006).

Although common among athletically trained horses, with a reported prevalence of 67% (Barr, Pinchbeck et al. 2009), the pathological changes associated with POD are difficult to detect clinically. It is physically impossible to view the POD lesion sites during routine arthroscopic examination (Barr, Pinchbeck et al. 2009), and only severe lesions are readily detectable on routine radiography (Richardson 2003). As a consequence, the lesions often remain undiagnosed until the late stages of disease, by which point the pathological changes are irreversible, resulting in chronic joint disease (Barr, Pinchbeck et al. 2009).

Microdamage accumulation due to excessive loading is the cause of another problem in the palmar metacarpal, this time located in the parasagittal grooves. This common condition, known as a parasagittal linear defect, can be found in approximately 75% of training and racing Thoroughbreds in the United Kingdom (Riggs, Whitehouse et al. 1999). The defects arise from the accumulation of microdamage which leads to a branching array of cracks in the subchondral bone of the parasagittal grooves (Radtke, Danova et al. 2003), and is associated with bone sclerosis induced by the cyclic loading experienced during training and racing (Reilly, Currey et al. 1997). These changes precede the formation of catastrophic fractures at this site (Radtke, Danova et al. 2003), and it has been suggested that these fractures are the result of a fatigue process leading to the growth of a single dominant crack from within the array of microdamage (Radtke, Danova et al. 2003). This larger scale parasagittal fracture is common during racing and training (Ellis 1994; Johnson, Stover et al. 1994) and is reported as accounting for approximately 25% of all catastrophic injuries among racing Thoroughbreds in California (Johnson, Stover et al. 1994). In fact, this type of fracture is one of the most frequent reasons for euthanasia (Rick, O'Brien et al. 1983; Stephens, Richardson et al. 1988).

Previous structural studies of damage accumulation in the palmar aspect of the equine MC3 can be broadly divided into three somewhat distinct categories: (i) gross examination (Radtke, Danova et al. 2003; Barr, Pinchbeck et al. 2009); (ii) focused microscopic assessment of specific structural features (Norrdin and Stover 2006; Boyde, Riggs et al. 2011); (iii) multi-scalar structural assessment (Norrdin, Kawcak et al. 1998) (Muir, Peterson et al. 2008). With respect to the substantial body of research noted above, there is still a need to understand at a detailed structural level how overload arthroses progress at this site, and in the context of the functionally integrated joint tissue complex (i.e. the articular surface, the hyaline and calcified cartilage and the subchondral bone).

The consistent occurrence of microdamage at the distal end of the equine MC3, makes it a valuable model for understanding structural changes in the subchondral bone and overlying cartilage associated with excessive mechanical loading. The aim of this new study was to provide a broad microstructural survey of the effects of microdamage accumulation in the palmar aspect of the equine MC3 condyles occuring in the hyaline and calcified cartilage, and the subchondral bone, and to map the progression of disease through the presentation of a broad range of pathological states.

METHODS

MC3 bones were collected from the right forelimb of 16 Thoroughbred racehorses that had been in active race training at the Hong Kong Jockey Club and required euthanasia over a period of 6 months from 2008-2009. The horses were between 3 and 8 years of age, and the number of race starts for each animal ranged

from 2 to 57. Clinical data indicated that one animal suffered a catastrophic fracture of the MC3, and two animals had suffered proximal sesamoid fractures, all in the non-sampled left forelimb.

The MC3 bones, having been stored frozen below -20°C, were defrosted in cold running water. The articular condyles were examined for gross defects using India ink staining to detect cartilage disruption, and then scored using an equine fetlock-specific grading system (Barr, Pinchbeck et al. 2009). Osteochondral slabs in the mediolateral plane, ~4mm thick, were sawn from both the lateral and medial condyles of the palmar aspect. These slabs were aligned perpendicularly to the joint surface, and inclined at ~35° to the line of the centre of the shaft, such that they passed through the centre of rotation of the distal MC3 (Figure 1). This site was selected because of its association with commonly formed lesions (Pool 1996) and the highest *in vivo* loads (Firth, Rogers et al. 2005) i.e. the contact site between the sesamoid bones and MC3 during the loading phase of high-speed locomotion (Stashak and Hill 2002).

Each osteochondral slab was chemically fixed in 10 % formalin for 1 week, and then mildly decalcified in 10 % formic acid for ≈5 days. Finally, cryo-sectioning was used to obtain relatively thick (≈30 µm) osteochondral sections which were viewed in a fully hydrated state using transmission bright field microscopy and differential interference contrast (DIC) microscopy. This microscopy was used to assess microdamage in two regions of interest: the parasagittal groove and the mid-condylar region.

RESULTS

Table 1 presents information relating to each horse's age, number of race starts, and a brief overview of their macro- and microscopic appearances. For the purposes of comparison we have defined the 'younger' age group as those horses 5 years and under. This distinction conveniently corresponded to a substantial increase in number of race starts, such that the younger animals had ≤12 race starts in comparison to their older counterparts with ≥21 race starts.

Macroscopic Examination

Macroscopically, the cartilage in the younger animals appeared generally intact, as indicated by India ink staining (Figures 2A & B). Typically there was only subtle evidence of wear lines (faintly visible only under oblique illumination); mild linear fissures in the parasagittal grooves characterised by slight roughening of the cartilage (see arrows in Figure 2A); and occasionally minor cartilage disruption associated with the transverse ridge. Of note was one MC3 that contained a distinct mid-condylar lesion (see arrowhead in Figure 2A) that was more opaque and slightly sunken in appearance relative to the surrounding cartilage. Another MC3 exhibited bruising beneath normal cartilage at the mid-condylar region of one condyle (see arrow in Figure 2B), with a further animal exhibiting much more subtle bruising. Although these two latter features were not representative of the younger animals, similar such lesions were seen with greater severity and frequency in older animals.

With increasing age the animals generally exhibited more definite wear lines and linear fissures in the parasagittal groove, and more extensive cartilage disruption associated with the transverse ridge (see arrows in Figures 2C & D). Cartilage disruption at the transverse ridge ranged from localised partial thickness ruptures, through to full thickness ulcerations up to ≈10 mm^2 in area, with the previously attached cartilage forming a 'flap' that partially covered the exposed hard tissue. In the mid-condylar region, moderate cartilage disruption and mild evidence of bruising was typical (e.g. see arrowheads in Figure 2C).

Microstructural Analysis

Microstructural analysis revealed varying degrees of microdamage in the calcified cartilage and subchondral bone in both the parasagittal groove and mid-condylar region. The damage in each of these regions was generally separated by an area of healthy tissue, and was often hidden beneath intact hyaline cartilage. A common feature of all samples was high subchondral bone density, particularly in the mid-condylar region where there was a near-complete absence of trabecular spaces to a depth of several millimetres subjacent to the cartilage (see Figure 3).

Microstrutural damage associated with the parasagittal groove

Microdamage was present in the parasagittal groove in animals of all ages. In the younger horses this damage consisted of occasional mid-sized cracks through the calcified cartilage (Figure 5), sometimes terminating in lesions in the deep zone hyaline cartilage (see arrows in Figures 4B & C). This damage was often accompanied by clusters of much smaller cracks in the subjacent bone (see boxed region in Figure 4B). Further, there was some evidence that intense microcracking in the calcified cartilage was linked with a localised area of lesser calcified cartilage thickness, giving the appearance of a recess in the tidemark (see arrows in Figure 5C).

With increasing age a greater intensity of subchondral bone damage was observed and the cracks in the calcified cartilage were generally larger and more numerous, and they more frequently penetrated into the hyaline cartilage (Figure 5). It should be noted that the cracks in both the subchondral bone and the calcified cartilage of the parasagittal groove were aligned at approximately 45° to the local articular surface, and at higher densities had an oblique/counter-oblique intersecting morphology, with cracks of varying sizes forming fractal arrays (see especially enlarged Figure 5C).

As also seen in the younger animals, where the cracks advanced across the most distal tidemark they were often associated with lesions in the hyaline cartilage. In the older animals these lesions were generally more pronounced, with some extending almost to the articular surface (Figures 5A & B). The hyaline cartilage matrix immediately adjacent to these lesions was clearly modified both in terms of cell clustering, acellularity and matrix alignment as indicated by the lines of chondrocyte continuity (Figure 5C). As in the younger animals, focal areas of lesser calcified cartilage thickness could occasionally be found in association with intense microdamage (Figure 5C).

Microstructural damage associated with the mid-condylar region

Of the 10 younger animals, 7 exhibited no significant microscopic evidence of damage in the mid-condylar region. There was no obvious microcracking of the calcified cartilage or subchondral bone, no articular surface disruption, and the hyaline cartilage matrix appeared normal (Figure 6). The remaining 3 younger animals (Horses 4, 5, 7) displayed notable lesions. In the older animals lesions were both more frequent and generally more severe, with 5 of the 6 animals displaying significant damage (Table 1). In both age groups two distinct types of lesion were identified.

The first type of lesion involved focal subchondral bone collapse, with the overlying hyaline cartilage folding into the resultant void in the subchondral plate (Figure 7). Additionally, a clearly discernable layer of “darker” tissue had formed at the articular surface (see Figure 7) that corresponds to the opaque cartilage observed macroscopically (Figure 2A). This “neo-tissue” was readily distinguishable from, yet structurally integrated with, the underlying hyaline cartilage. Higher magnification imaging (Figure 7B) indicated that it was highly fibrous in nature and devoid of chondrocytes. No such neo-tissue was seen in the other younger animals.

A more severe lesion of the same type as that shown in Figure 7 was also found in the older animals. This lesion is identified macroscopically in the boxed region shown in Figure 2D and its microstructural features are shown in Figure 8. Severe subchondral bone collapse is visible on the left (Figure 8A) with the resultant void having been partially filled by both cartilage infolding and loose cartilage and bone fragments. Another region of subchondral subsidence is evident on the right in Figure 8A, this time appearing more stable, with the subchondral bone on the extreme right remaining largely intact. The subchondral bone adjacent to these sites shows considerable evidence of microdamage accumulation, with the oblique/counter-oblique microcracks appearing to have progressed such that the bone in the central-most region has a comminuted appearance (shown enlarged in Figure 8B). Both sites of subsidence were associated with an abnormal thickening of the overlying hyaline cartilage, with regions of contrasting neo-tissue having formed at the articular surface. This tissue varied somewhat in its microstructure: in some regions it had a fibrous texture with a distinct boundary separating it from the hyaline cartilage, similar to that seen in the younger animals (see Figure 7B); in other regions the fibrous structure appeared less organised and blended more gradually into the underlying hyaline cartilage (see Figure 8C). Examples of similar such neo-tissue tissue were found in 3 of the 6 older animals.

The second of the two mid-condylar lesions noted in the 3 younger animals exhibited obvious subchondral damage spread across a large area (Figure 9), and corresponded to macroscopically observed bruising (as in Figure 2B). The subchondral bone microcracks in this region are chaotic, exhibiting less clearly the oblique/counter-oblique morphology noted earlier. Further, microcrack coalescence has resulted in the formation of a larger laterally-spreading fracture in the subchondral plate (see region arrows in Figure 9).

An example of a lesion of the same type from an older animal (Figure 10) shows more advanced crack coalescence leading to a much larger lateral fracture. One end of this large fracture breaches the distal-most tidemark and is associated with a distortion of the hyaline cartilage matrix (see enlarged view in Figure 10B). At the lesion periphery the typical oblique/counter-oblique crack morphology is present (see arrowed site in Figure 10B), while directly subjacent to the lateral fracture the bone has a comminuted appearance (see enlarged image in Figure 10C). Examples of this type of mid-condylar lesion seen in both the younger and older animals were always associated with a macroscopically visible bruising beneath the articular cartilage. Addititionally, this lesion was associated with the formation of fibrous neo-tissue at the articular surface (Figure 10A) with a very similar appearance to that observed in the younger animal (Figure 7).

Finally, a clear example of a tidemark recess was found in the mid-condylar region (Figure 11), similar to that seen in the parasagittal groove.

DISCUSSION

Microdamage accumulation, due to repetitive overloading, is a common problem affecting the palmar aspect of the distal end of the MC3 of Thoroughbreds athletes (Pool 1996; Radtke, Danova et al. 2003). In this study a range of microdamage severity was observed in two clinically important sites, the parasagittal groove and the mid-condylar region, with a general trend of increasing levels of damage with increasing animal age. This has enabled us to investigate the general morphological progression of damage arising from repetitive overloading in the joint of a large athletic animal.

Overall, in both the parasagittal groove and mid-condylar region there was a trend towards increasing intensity of microcracking (in terms of both crack number and size) in the calcified cartilage and subchondral bone as animal age increased (cf. Figures 4 & 5; 7 & 8; 9 & 10). Especially noticeable at high crack densities was a distinct oblique/counter-oblique crack morphology, which is characteristic of failure

occurring along the planes of maximum shear stress orientated at ~45° to the principal loading axis. In a congruent joint this axis would be approximately normal to the articular surface. It would appear that accumulation of these oblique/counter oblique microcracks, which form fractal arrays, lead eventually to the comminuted appearance of the subchondral bone seen in the severe mid-condylar lesions in the older animals (see Figures 8B and 10C).

All of the 10 younger horses had microdamage in the parasagittal groove, whereas only 3 had detectable damage in the mid-condylar region (see Table 1). This contrasts with the 6 older horses where both parasagittal and mid-condylar damage were detected in all but one case. This suggests that microdamage development in the parasagittal groove precedes that in the mid-condylar region. Additionally, in the younger animals damage in the calcified cartilage of the parasagittal groove was noticeably more severe than that in the underlying subchondral bone (Figure 4), suggesting a predispostition to failure in the calcified cartilage at this site. Indeed, for all ages of animal, microcracking of the calcified cartilage was typically of greater intensity in the parasagittal groove than in the mid-condylar region, where cracks in the calcified cartilage were relatively infrequent even in the presence of severe subchondral bone damage (see Figures 8B, 9, 10C). This apparent predisposition to microdamage of the calcified cartilage in the parasagittal groove is most likely due to differences in loading conditions between the two sites. Further, evidence that this hard tissue microdamage might interfere with the normal calcification process is provided by the pronounced recesses observed in the most distal tidemark of the ZCC in the regions of intense microcracking (see Figures 4C, 5C, 11).

The close association between lesions in the hyaline cartilage and microdamage in both the subchondral bone and calcified cartilage across the entire age spectrum (see Figures 4 and 5) suggests that hard tissue fracture that impinges directly on the deep-zone hyaline cartilage leads to some form of reactive response in the cartilage with subsequent lesion formation. Additionally, these cartilage lesions bear some resemblance, in both morphology and location, to previously described extrusions of mineralised matrix (Boyde, Riggs et al. 2011). Although our imaging technique did not allow us to determine whether or not the contents of the lesions in the hyaline cartilage (e.g. Figure 5A) were mineralised, it is conceivable that they may represent a related form of pathology. Further, where these lesions were associated with voids (see Figure 4B) they may well have resulted from the artefactual loss of mineralised fragments during preparation.

The microdamage detected in the parasagittal groove correlates well with previous macroscopic observations of subchondral cracking in this region, in terms of both extent and gross morphology (Riggs, Whitehouse et al. 1999; Radtke, Danova et al. 2003). Further, the hard tissue and hyaline cartilage lesions described in the present study appear to correspond to the parasagittal linear fissures reported elsewhere (Riggs, Whitehouse et al. 1999; Barr, Pinchbeck et al. 2009). The observed increase in microcrack density with increasing animal age (and number of race starts) supports the suggestion that these lesions develop via a process of fatigue (Riggs, Whitehouse et al. 1999; Riggs 2002; Radtke, Danova et al. 2003), and may progress eventually to the catastrophic condylar fractures documented at this site (Ellis 1994; Zekas, Bramlage et al. 1999).

The microdamage in the mid-condylar region, while having many morphological features in common with those observed in the parasagittal groove, differed significantly in the type and severity of lesion developed. The mid-condylar region of younger horses typically lacked any visible sign of damage (Figure 6), with the very dense subchondral bone being the only evidence of high *in vivo* loading (Figure 3). The few lesions that were present in the younger animals appeared to correspond to similar but more advanced lesions in the older animals (c.f. Figures 7 & 8; 9 & 10). In these older animals the mid-condylar lesions were frequently of greater severity and more extensive than those in the parasagittal groove (c.f. Figures 5 & 8),

which suggests that although damage in the parasagittal groove generally develops at an earlier stage, lesions in the mid-condylar region often progress to a more advanced state.

While severe subchondral bone damage in the mid-condylar region often occurred with no visible damage to the overlying articular surface (see Figures 9 and 10), eventually the hard tissue damage appears to escalate such that the deep hyaline cartilage is compromised. For example, the RH extremity of the main coalesced crack in Figure 10A has penetrated the calcified cartilage and hyaline cartilage to create what appears to be an incipient cartilage lesion (enlarged in Figure 10B). More severe examples are shown in Figure 8A where subchondral bone collapse has caused the hyaline cartilage to fold inwards into a void in the subchondral plate. The fibrous "neo-tissue" at the articular surface at these sites of cartilage infolding (see Figure 7; arrowed sites in Figure 8A; Figure 8C) appears to be reparative in nature, and would help to maintain congruency in the joint following the collapse of the subjacent subchondral bone. Our microstructural evidence indicates that this reparative tissue differs structurally, and perhaps even materially, from the original hyaline cartilage (see Figures 7B and 8C), but its exact nature remains unclear.

The changes observed in the mid-condylar region were characteristic of palmar osteochondral disease (Pool 1996; Norrdin, Kawcak et al. 1998; Barr, Pinchbeck et al. 2009) and consistent with reports of similar lesions involving subchondral bone loss with associated cartilage damage (Riggs, Whitehouse et al. 1999) and infolding of hyaline cartilage following subchondral collapse (Norrdin, Kawcak et al. 1998; Muir, Peterson et al. 2008). The high level of hard tissue microdamage that was often found beneath regions of intact hyaline cartilage (Figures 8, 9 & 10) supports the idea that significant disruption to the subchondral bone precedes cartilage degeneration in the development of these lesions (Riggs, Whitehouse et al. 1999), and also provides further evidence for the development of these lesions by a process of fatigue (Pool 1996). Further, our study provides additional evidence that the mid-condylar lesions are anatomically independent of those in the parasagittal groove (Pool and Meagher 1990; Pool 1996), being spatially and often temporally distinct. This is an important point when considering the pathogenesis of condylar fractures.

It is important to note that much of the subchondral damage observed in this study was only subtly apparent from external examination of the joint surface. Outwardly intact hyaline cartilage often masked significant hard tissue microdamage in both the parasagittal groove and the mid-condylar region (e.g. Figures 5A & 9), and even in cases of significant disruption to the cartilage (i.e. subchondral collapse, see Figures 7 & 8), the formation of fibrous neo-tissue concealed the full extent of the injury. Additionally, mild bruising of the subchondral bone, barely visible through the intact cartilage, corresponded to moderately high levels of hard tissue microdamage (Figures 9 & 10).

To conclude, this study has provided a detailed, micro-level insight into the progression of repetitive overload arthrosis in the palmar aspect of the third metacarpal of the equine athlete. The study has identified extensive levels of hard tissue microdamage concealed beneath the outwardly intact hyaline cartilage, and revealed the progression from initial microcrack formation through to severe subchondral bone collapse and lesion formation in the hyaline cartilage.

ACKNOWLEDGEMENTS

The authors would like to thank the Equine Trust (NZ) for their generous financial support. Additionally, the authors are grateful to both Dr Chris Riggs (Department of Veterinary Clinical Services, Hong Kong Jockey Club) and Professor Elwyn Firth (Department of Sport and Exercise Science, The University of Auckland) for their work in providing the trained racehorse tissue and horse histories, without which this work would not have been possible.

REFERENCES

Barr, E. D., G. L. Pinchbeck, et al. (2009). "Post mortem evaluation of palmar osteochondral disease (traumatic osteochondrosis) of the metacarpo/metatarsophalangeal joint in Thoroughbred racehorses." Equine Veterinary Journal **41**(4): 366-371.

Biewener, A. A. (1993). "Safety factors in bone strength." Calcified Tissue International **53**(SUPPL. 1): S68-S74.

Biewener, A. A., J. Thomason, et al. (1983). "Bones stress in the horse forelimb during locomotion at different gaits: A comparison of two experimental methods." Journal of Biomechanics **16**(8): 565-576.

Boyde, A., C. M. Riggs, et al. (2011). "Cartilage damage involving extrusion of mineralisable matrix from the articular calcified cartilage and subchondral bone." European Cells and Materials **21**: 470-478; discussion 478.

Burr, D. B. and E. L. Radin (2003). "Microfractures and microcracks in subchondral bone: Are they relevant to osteoarthrosis?" Rheumatic Disease Clinics of North America **29**(4): 675-685.

Ellis, D. R. (1994). "Some observations on condylar fractures of the third metacarpus and third metatarsus in young thoroughbreds." Equine Veterinary Journal **26**(3): 178-183.

Firth, E. C., C. W. Rogers, et al. (2005). "Musculoskeletal responses of 2-year-old Thoroughbred horses to early training. 6. Bone parameters in the third metacarpal and third metatarsal bones." New Zealand Veterinary Journal **53**(2): 101-112.

Frost, H. M. (1994). "Perspectives: A biomechanical model of the pathogenesis of arthroses." Anatomical Record **240**(1): 19-31.

Johnson, B. J., S. M. Stover, et al. (1994). "Causes of death in racehorses over a 2 year period." Equine Veterinary Journal **26**(4): 327-330.

Martin, R. B., S. M. Stover, et al. (1996). "In vitro fatigue behavior of the equine third metacarpus: Remodeling and microcrack damage analysis." Journal of Orthopaedic Research **14**(5): 794-801.

Mori, S., R. Harruff, et al. (1993). "Microcracks in articular calcified cartilage of human femoral heads." Archives of Pathology and Laboratory Medicine **117**(2): 196-198.

Muir, P., A. L. Peterson, et al. (2008). "Exercise-induced metacarpophalangeal joint adaptation in the Thoroughbred racehorse." Journal of Anatomy **213**(6): 706-717.

Norrdin, R. W., C. E. Kawcak, et al. (1998). "Subchondral bone failure in an equine model of overload arthrosis." Bone **22**(2): 133-139.

Norrdin, R. W. and S. M. Stover (2006). "Subchondral bone failure in overload arthrosis: A scanning electron microscopic study in horses." Journal of Musculoskeletal Neuronal Interactions **6**(3): 251-257.

Pool, R. R. (1996). Pathologic manifestations of joint disease in the athletic horse. Joint disease in the horse. C. W. McIlwraith and G. W. Trotter. Philadelphia, W.B. Saunders**:** 87-104.

Pool, R. R. and D. M. Meagher (1990). "Pathologic findings and pathogenesis of racetrack injuries." The Veterinary Clinics of North America. Equine Practice **6**(1): 1-30.

Radin, E. L., H. G. Parker, et al. (1973). "Response of joints to impact loading - III. Relationship between trabecular microfractures and cartilage degeneration." Journal of Biomechanics **6**(1).

Radtke, C. L., N. A. Danova, et al. (2003). "Macroscopic changes in the distal ends of the third metacarpal and metatarsal bones of Thoroughbred racehorses with condylar fractures." American Journal of Veterinary Research **64**(9): 1110-1116.

Reilly, G. C., J. D. Currey, et al. (1997). "Exercise of young thoroughbred horses increases impact strength of the third metacarpal bone." Journal of Orthopaedic Research **15**(6): 862-868.

Richardson, D. W. (2003). The metacarpophalangeal joint. Diagnosis and Management of Lameness in the Horse. M. W. Ross and S. J. Dyson, W. B. Saunders**:** 348-362.

Rick, M. C., T. R. O'Brien, et al. (1983). "Condylar fractures of the third metacarpal bone and third metatarsal bone in 75 horses: radiographic features, treatments, and outcome." Journal of the American Veterinary Medical Association **183**(3): 287-296.

Riggs, C. M. (2002). "Fractures - A preventable hazard of racing thoroughbreds?" Veterinary Journal **163**(1): 19-29.

Riggs, C. M. (2006). "Osteochondral injury and joint disease in the athletic horse." Equine Veterinary Education **18**(2): 100-112.

Riggs, C. M., G. H. Whitehouse, et al. (1999). "Pathology of the distal condyles of the third metacarpal and third metatarsal bones of the horse." Equine Veterinary Journal **31**(2): 140-148.

Schaffler, M. B., E. L. Radin, et al. (1989). "Mechanical and morphological effects of strain rate on fatigue of compact bone." Bone **10**(3): 207-214.

Sokoloff, L. (1993). "Microcracks in the calcified layer of articular cartilage." Archives of Pathology and Laboratory Medicine **117**(2): 191-195.

Stashak, T. S. and C. Hill (2002). Conformation and movement. Adams' Lameness in Horses. T. S. Stashak**:** 82.

Stephens, P. R., D. W. Richardson, et al. (1988). "Slab fractures of the third carpal bone in standardbreds and thoroughbreds: 155 cases (1977-1984)." Journal of the American Veterinary Medical Association **193**(3): 353-358.

Zekas, L. J., L. R. Bramlage, et al. (1999). "Characterisation of the type and location of fractures of the third metacarpal/metatarsal condyles in 135 horses in central Kentucky (1986-1994)." Equine Veterinary Journal **31**(4): 304-308.

Zioupos, P. and J. D. Currey (1994). "The extent of microcracking and the morphology of microcracks in damaged bone." Journal of Materials Science **29**(4): 978-986.

Table 1: A summary of history and microdamage in the mid-condylar region and parasagittal groove (PSG) for each horse. Younger and older animals separated by bold line. Description of microdamage grades provided below.

	History		Microdamage	
Horse	**Age**	**Race starts**	**Mid-Condylar**	**PSG**
1	3	2	None	Mild
2	3	7	None	Moderate
3	4	3	None	Mild
4	4	5	Moderate	Mild
5	4	6	Moderate	Mild
6	4	6	None	Mild
7	4	9	Moderate	Mild
8	5	8	None	Mild
9	5	8	None	Severe
10	5	12	None	Mild
11	6	21	Moderate	Moderate
12	6	27	Moderate	Mild
13	7	27	Severe	Severe
14	7	50	Severe	Moderate
15	8	56	Severe	Severe
16	8	57	Mild	Moderate

Mid-Condylar	
Mild	Few visible cracks, little/no disruption of overlying cartilage.
Moderate	May show evidence of an extensive network of subchondral microcracking, showing early signs of lateral fracture formation. Highly localised subchondral collapse. Overlying cartilage is undisrupted or suffers relatively minor disruption.
Severe	Evidence of extensive subchondral micro-cracking, involving one or more of bone comminution, lateral fracture, and subchondral collapse. Typically significant disruption of overlying cartilage, often accompanied by reparative tissue at the articular surface.

Parasagittal Groove	
Mild	Occasional cracks in the calcified cartilage, predominately slopping towards the sagittal ridge, sometimes associated with subtle subchondral bone damage.
Moderate	Frequent cracks in both the calcified cartilage and subchondral bone, typically exhibiting an oblique/counter-oblique morphology.
Severe	Extensive cracking of the calcified cartilage and subchondral bone with the formation of large cartilage lesions in association with the hard tissue macrodamage.

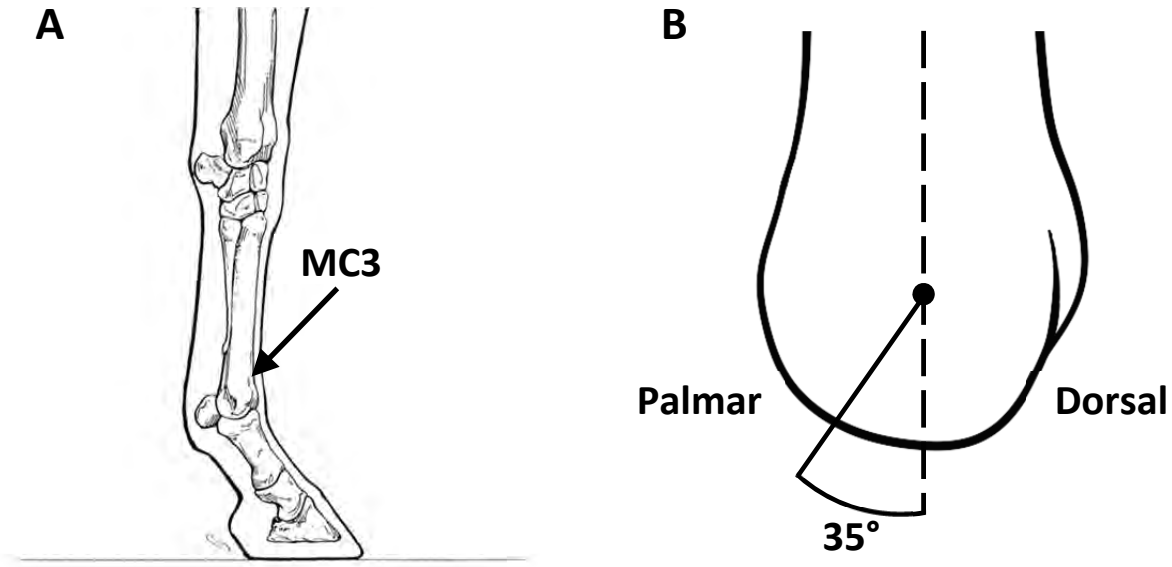

Figure 1: Schematics demonstrating sampling location. **(A)** Schematic showing the MC3 in context of the equine forelimb. **(B)** Schematic of the distal end of MC3, viewed in the medio-lateral plane, indicating the region of interest in the palmar aspect, the black dot in the centre representing an approximation of the centre of rotation of the distal MC3.

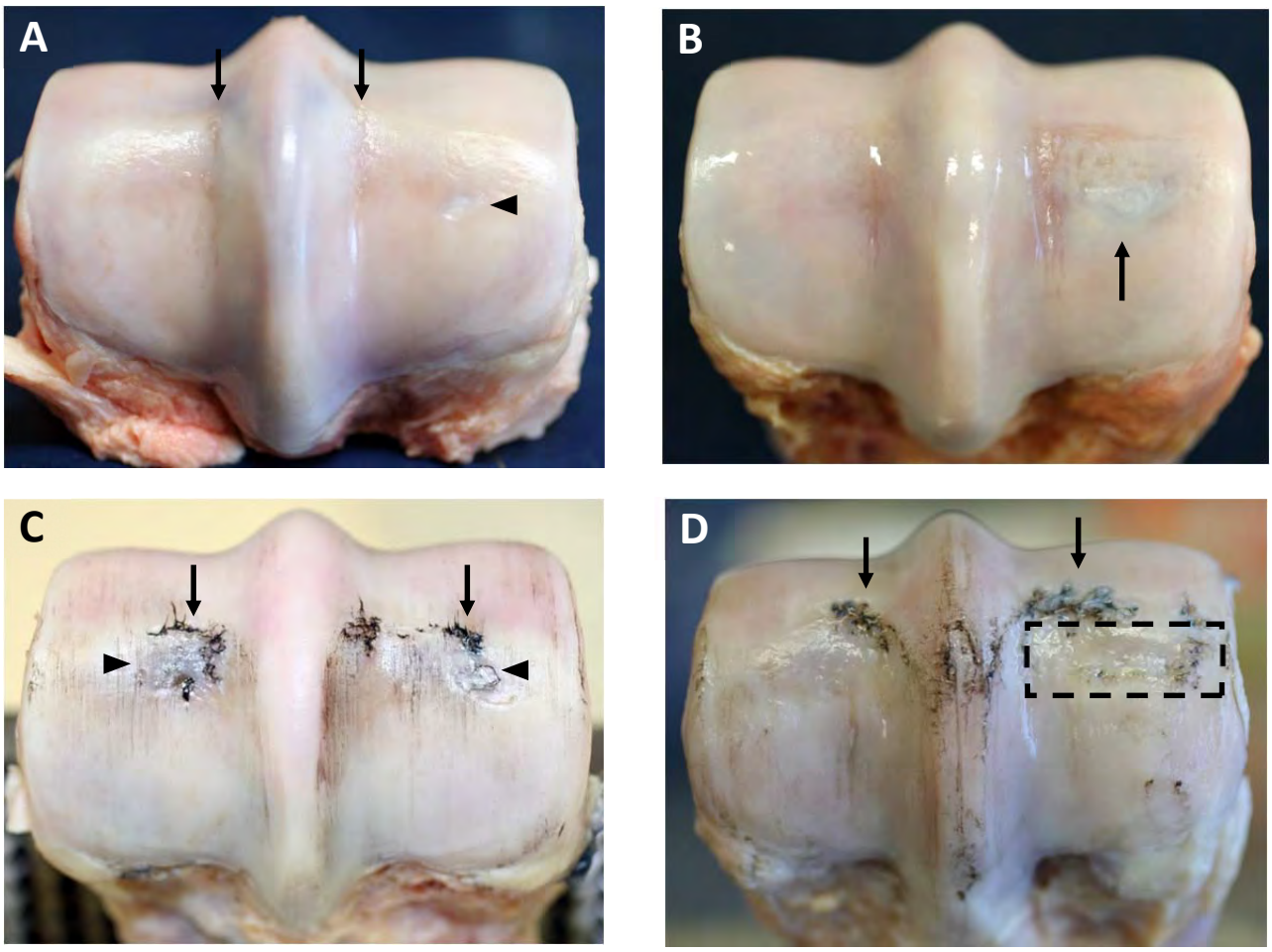

Figure 2: Macroscopic images of the distal end of the MC3 from younger (A & B) and older (C & D) animals. **(A)** Horse 5 showing an intact cartilage surface except for very slight linear fissures in the parasagittal grooves (see arrows). Note the small oval shaped area of opaque white cartilage visible in the centre of the medial condyle region (see arrowhead). **(B)** Horse 4 with arrow indicating a slightly darkened region beneath undisrupted cartilage. **(C)** Horse 14 showing minor wear lines, significant disruption at the transverse ridges (see arrows), and some darkening beneath the cartilage in the central condylar regions (see arrowheads), especially laterally. **(D)** Horse 13 showing a further example of cartilage disruption at the transverse ridge and mild articular surface roughening in the mid-condylar region (boxed region).

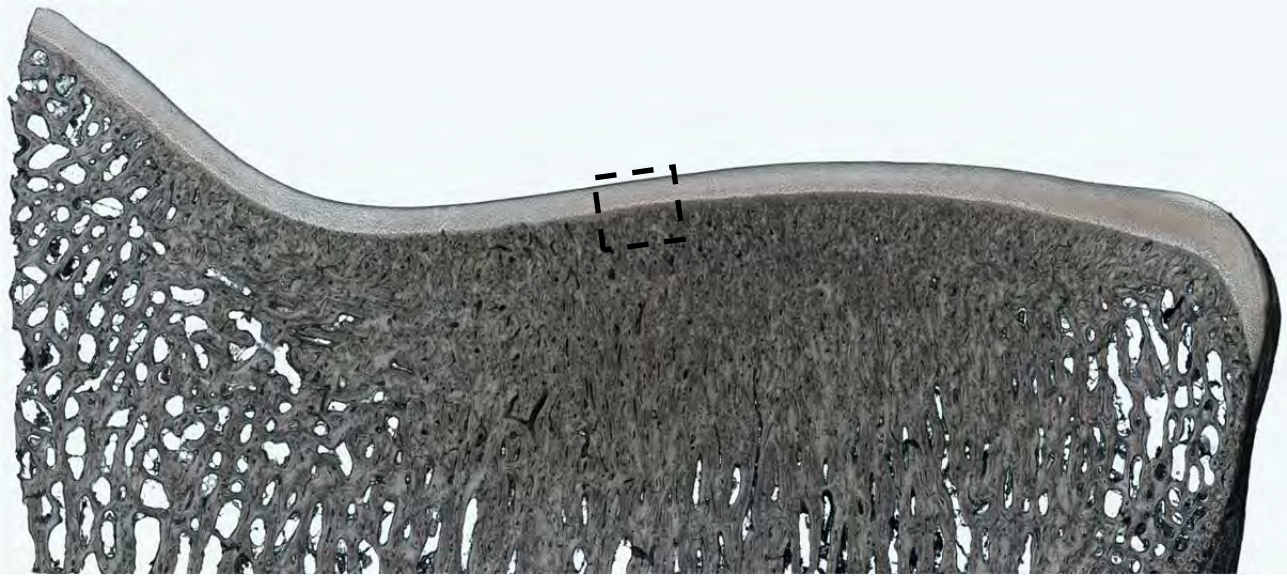

Figure 3: Horse 8 showing high subchondral bone density beneath the mid-condylar region and extending to a lesser degree into the parasagittal groove. Boxed region is enlarged in Figure 6.

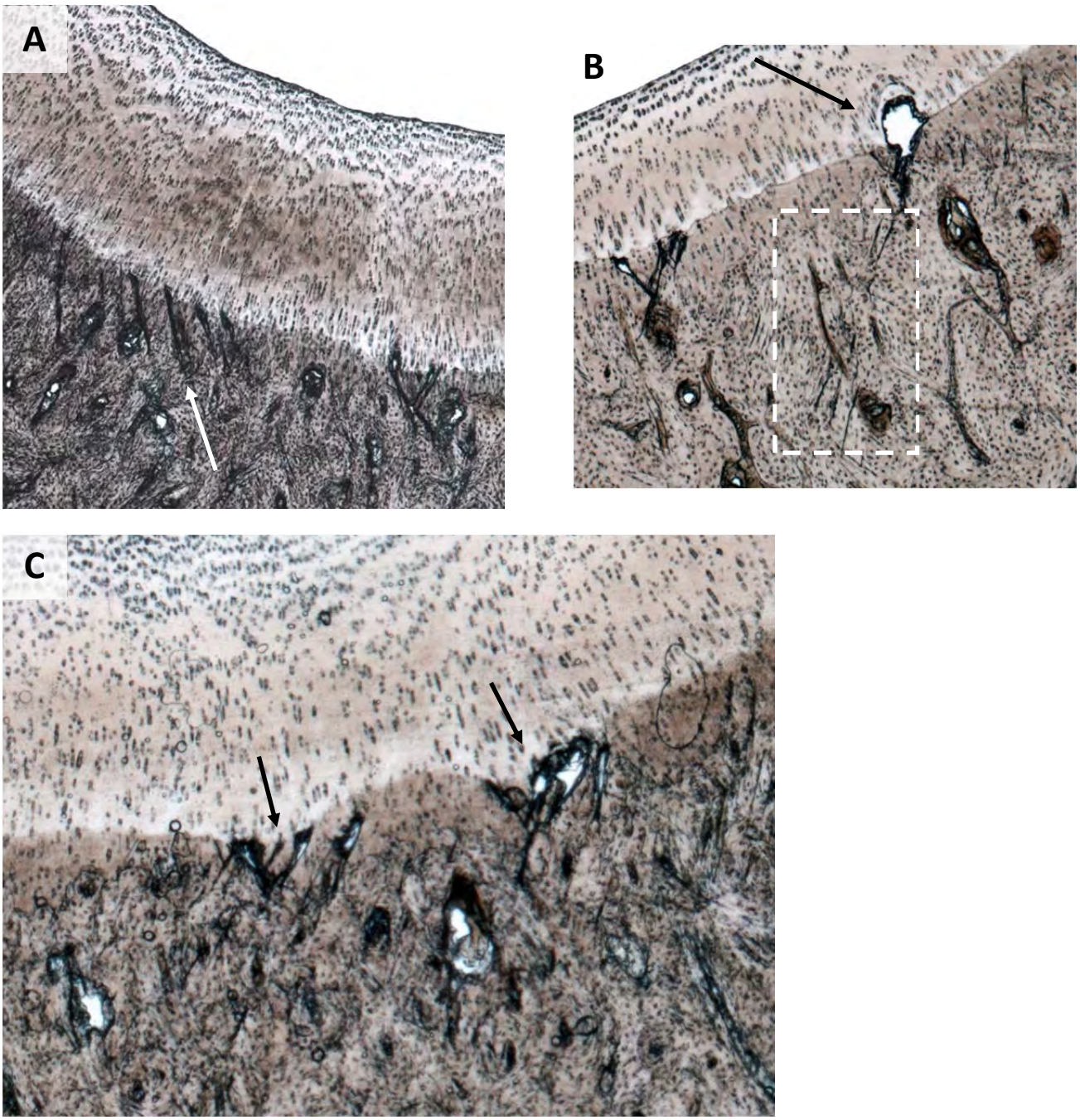

Figure 4: Examples of microdamage in the parasagittal groove of younger horses. **(A)** Horse 1 showing a cluster of obliquely aligned calcified cartialge microcracks beneath intact hyaline cartilage. **(B)** Horse 5 showing microcracks associated with lesion formation in the overlying hyaline cartilage (see arrow). Note also the more subtle but similarly aligned cracks in the subchondral bone (see boxed region). **(C)** Horse 6 showing two distinct recesses in the calcified cartilage closely associated with microdamage (see arrows), as well as small lesions (voids) at the same locations.

A

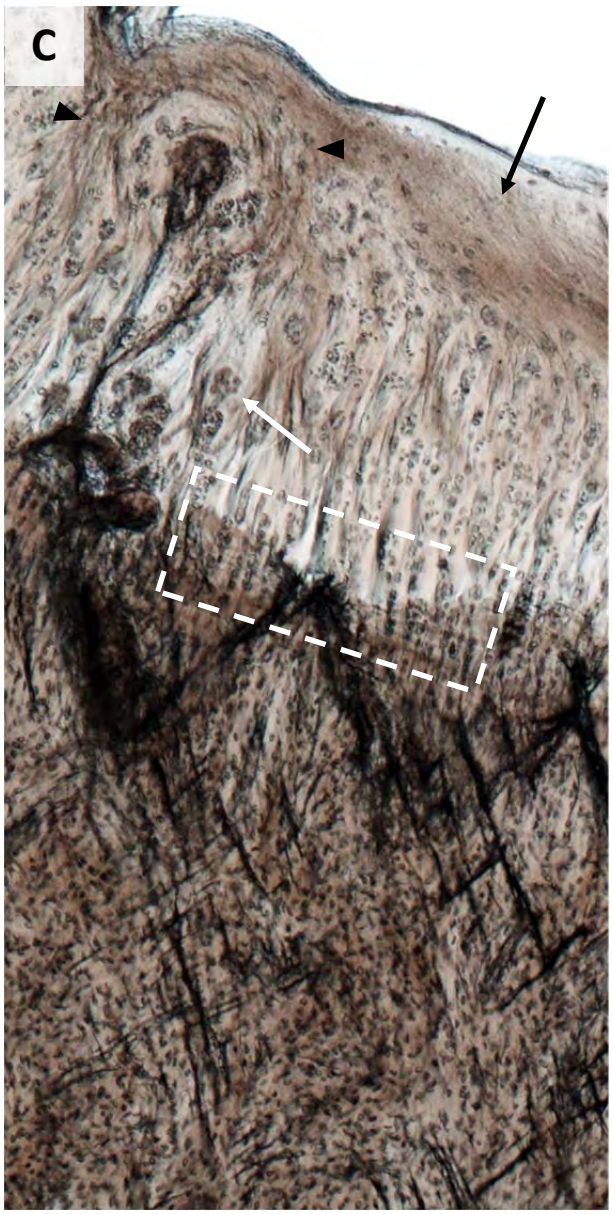

Figure 5: Horse 13 showing lesions in the hyaline cartilage and extensive microdamage in **(A)** the lateral and **(B)** the medial parasagittal groove. Note the high density of microcracks aligned in a cross-hatch configuration, with many large cracks extending across the calcified cartilage layer. **(C)** Enlarged image of the boxed region in (B). A number of changes can be seen in the hyaline cartilage including cell clustering (white arrow), regions of acellularity (black arrow), and regions of altered chondrocyte alignment suggestive of matrix remodelling (see black arrow heads). Cracks of various sizes can be seen in the subchondral bone.

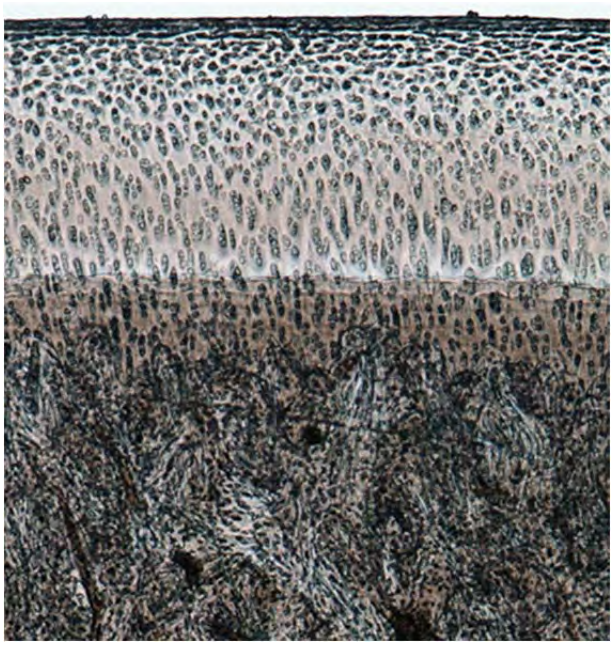

Figure 6: Higher magnification of boxed region in Figure 3, showing undamaged hyaline and calcified cartilage, and subchondral bone in the midcondylar region for the young Horse 8.

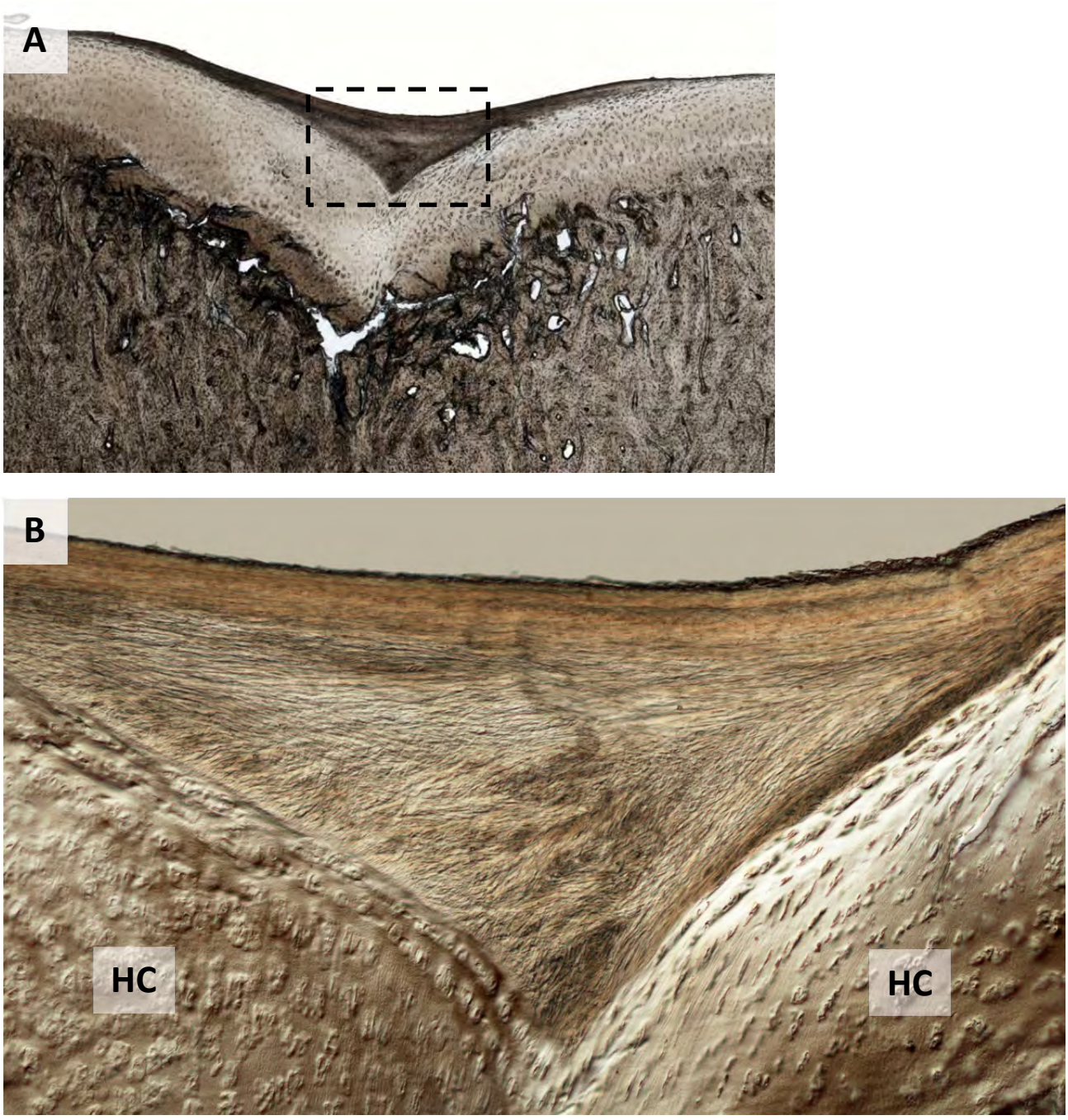

Figure 7: Horse 5 showing the example of the first observed lesion type in a younger animal. **(A)** Low magnification view showing subchondral bone collapse and cartilage infolding in the mid-condylar region. Note the contrasting layer of "neo-tissue" at the articular surface. **(B)** Higher magnification DIC image of the boxed region in (B). The neo-tissue that has formed is more fibrous in appearance and devoid of chondrocytes, thus being easily distinguished from the hyaline cartilage (HC) beneath, with which it is structurally integrated.

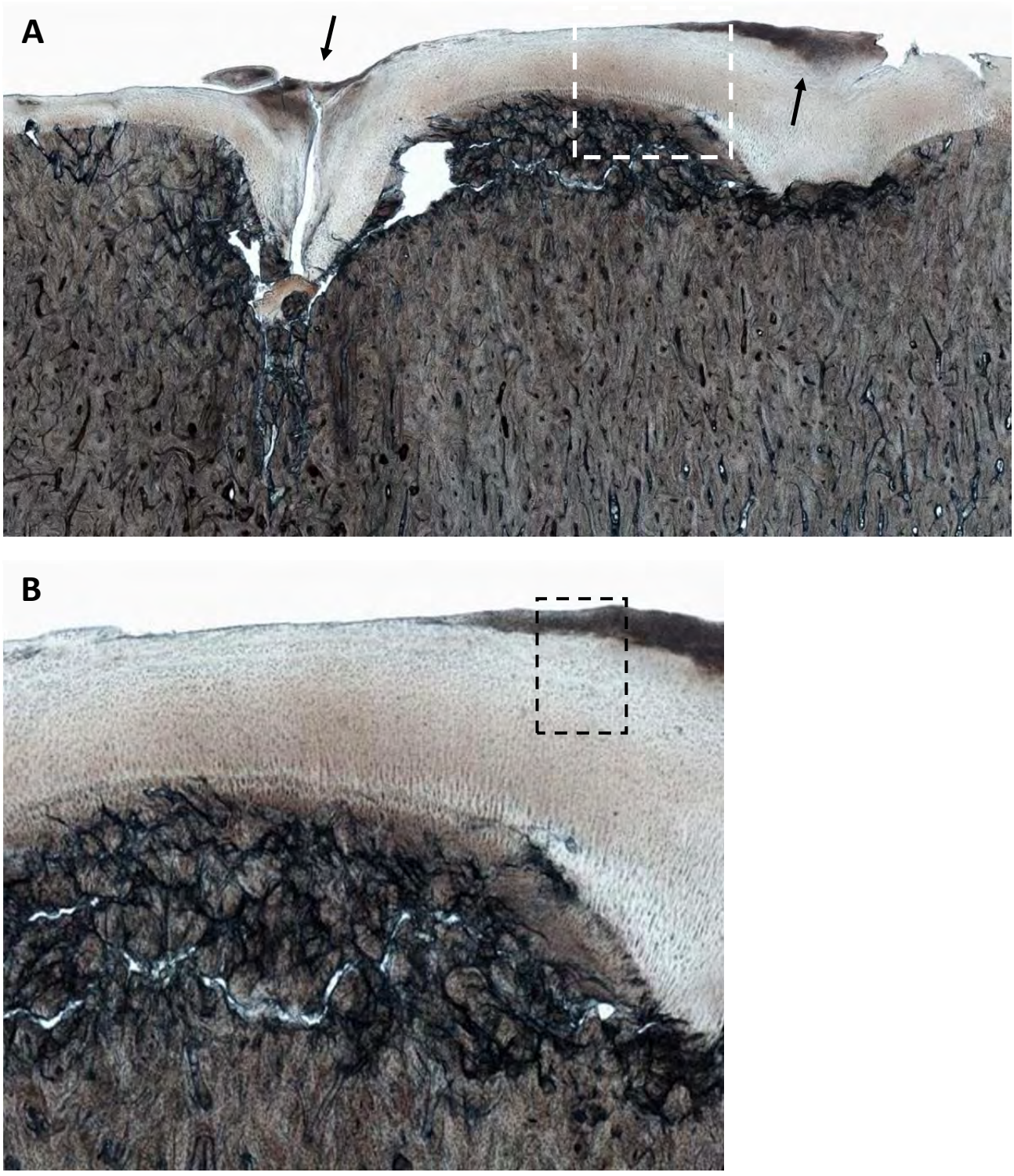

Figure 8: Horse 13 showing severe damage in the mid-condylar region. **(A)** Low magnification image. Subchondral bone collapse can be seen on the left with cartilage infolding. On the extreme right of the image there is evidence of what appears to be earlier subchondral collapse that may have stabilised. In both cases there is a greater amount of cartilage present than would be expected in a healthy region of the joint, with darker regions of neo-tissue at the articular surface (see arrows). The subchondral bone between the two collapsed regions has a comminuted appearance. **(B)** Enlarged view of boxed region in (A) showing severe damage in the subchondral bone, which as a result has a comminuted appearance.

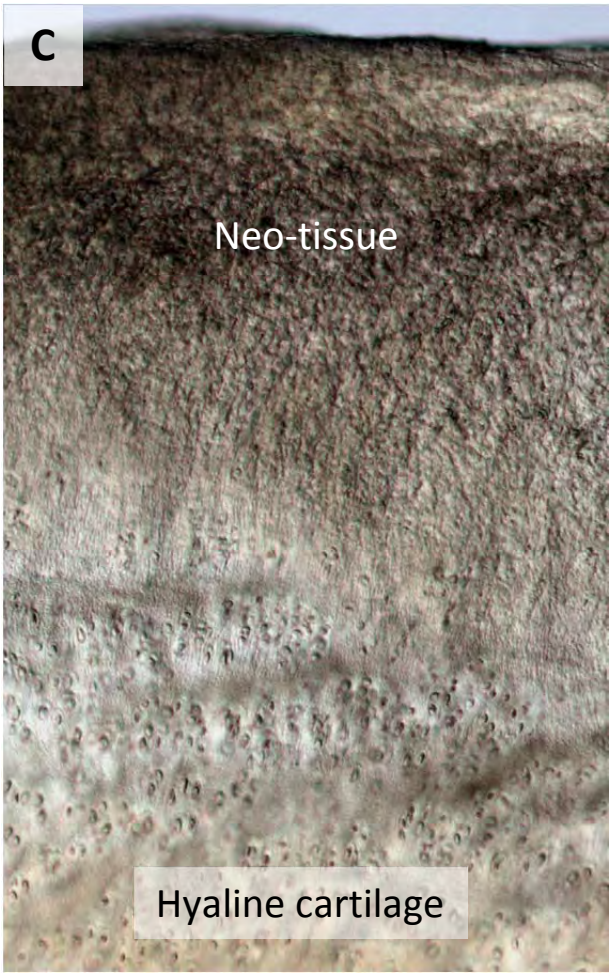

Figure 8C: Enlarged view of boxed region in Figure 8B showing the fibrous neo-tissue blending into the underlying hyaline cartilage.

Figure 9: Horse 4 showing accumulation of substantial microdamage in the subchondral bone beneath intact hyaline cartilage. Note coalescence of smaller cracks into a larger lateral fracture whose span is indicated by the white arrows.

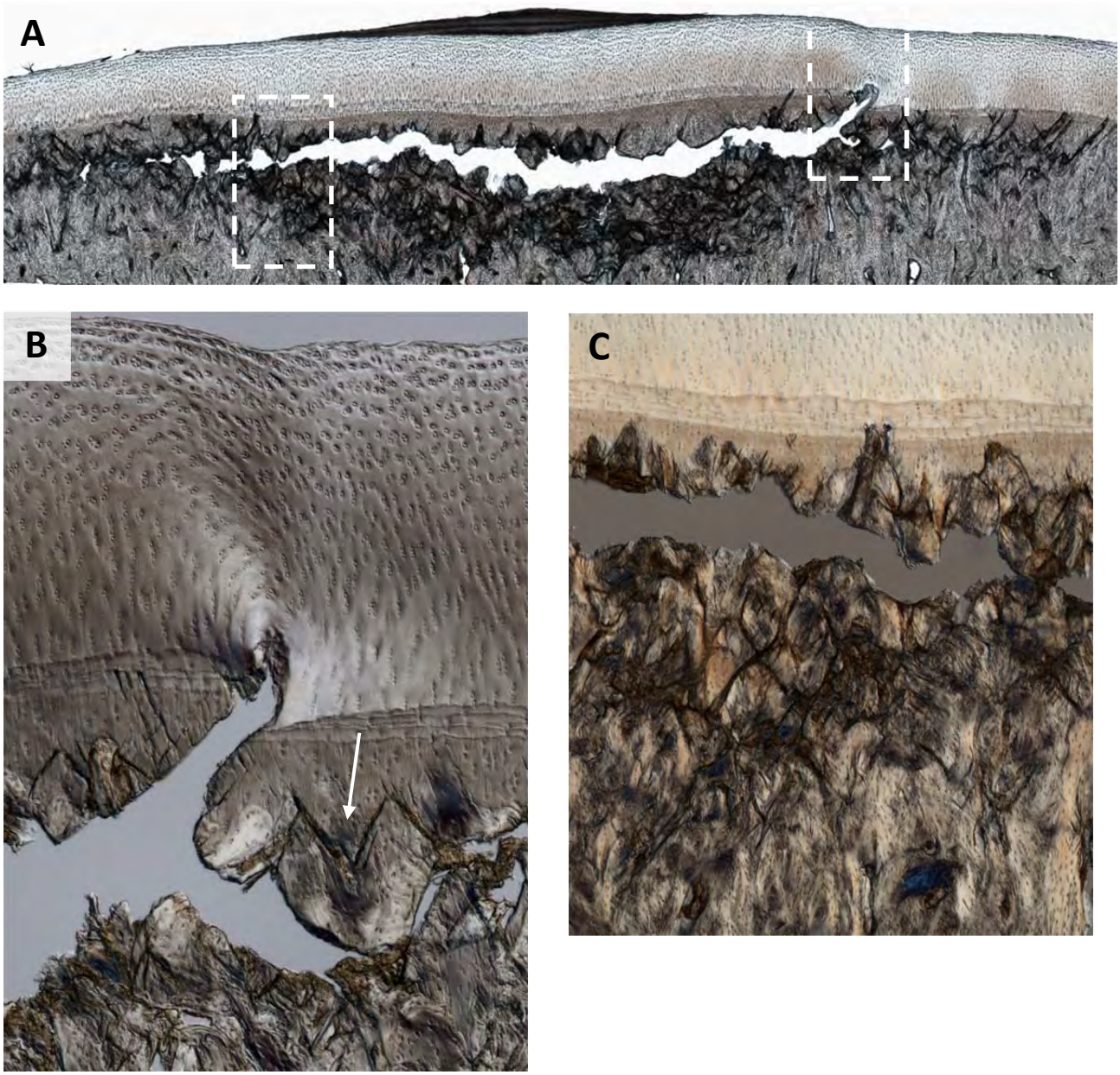

Figure 10: Horse 14 showing severe subchondral bone failure in the mid-condylar region. **(A)** Low magnification image. The bone at the centre of the lesion has a comminuted appearance, with less intense damage accumulation at the periphery. A large subchondral fracture can be seen subjacent to the calcified cartilage region, which at the right of the image penetrates all through to the deep articular cartilage (see RH boxed region). The articular surface is intact, though a layer of fibrous neo-tissue has formed above the centre of the lesion. **(B)** Enlarged view of RH boxed region in (A) showing failure of the calcified cartilage and penetration of the large crack into the hyaline cartilage. Note also the oblique/counter-oblique cracking of the subchondral bone (see arrow). **(C)** Image showing enlarged view of comminuted subchondral bone from same lesion site as indicated by the LH boxed region in (A).

Figure 11: Horse 14 showing a calcified cartilage recess in mid-condylar region of associated with microcracking.